Med Chem Res
DOI 10.1007/s00044-016-1648-1

MEDICINAL CHEMISTRY RESEARCH

ORIGINAL RESEARCH

1*H*-benzimidazole derivatives as butyrylcholinesterase inhibitors: synthesis and molecular modeling studies

Gunes Coban[1] · Luca Carlino[2] · Ayse Hande Tarikogullari[1] · Sülünay Parlar[1] · Görkem Sarıkaya[1] · Vildan Alptüzün[1] · Ayşe Selcen Alpan[1] · Hasan Semih Güneş[1] · Erçin Erciyas[1]

Received: 15 July 2015 / Accepted: 4 July 2016

Abstract A series of *N*-{2-[2-(1*H*-benzimidazole-2-yl) phenoxy]ethyl} substituted amine derivatives were synthesized and tested for their cholinesterase inhibitor activity. Acetylcholinesterase and butyrylcholinesterase inhibitor activities were evaluated in vitro by using Ellman's method. According to the activity results, all of the compounds displayed moderate acetylcholinesterase inhibitory activity and most of the compounds displayed remarkable butyrylcholinesterase inhibitory activity. Compound **3d** was the most active compound in the series and also a selective butyrylcholinesterase inhibitor. Molecular docking studies and molecular dynamic simulations were also carried out.

Keywords Alzheimer's disease · 1*H*-Benzimidazole · Acetylcholinesterase inhibitor · Butyrylcholinesterase inhibitor · Ellman's method · Molecular modeling

Abbreviations

AD	Alzheimer's disease
ACh	acetylcholine
AChE	acetylcholinesterase
AChEI	acetylcholinesterase inhibitor
ATC	acetylthiocholine iodide
BTC	butyrylthiocholine iodide
BuChE	butyrylcholinesterase
BuChEI	butyrylcholinesterase inhibitor
CAS	catalytic active site
ChE	cholinesterase
ChEI	cholinesterase inhibitor
DMF	dimethyl formamide
DMSO	dimethylsulfoxide
DTNB	5,5-dithiobis(2-nitrobenzoic acid)
HMBC	Heteronuclear Multiple Bond Correlation
HSQC	Heteronuclear Single Quantum Correlation
MD	molecular dynamics
RMSD	root main square deviation
TLC	thin-layer chromatography
VMD	visual molecular dynamics

Introduction

Alzheimer's disease (AD), the most common cause of dementia in elder, is a progressive neurodegenerative disorder characterized by loss of memory and cognition. 5.2 million people in the United States are suffering from AD and the number of patients increases every year, worldwide (Han and Mook-Jung, 2014; Thies and Bleiler, 2013). This disease is characterized by formation of cortical amyloid plaques and neurofibrillary tangles and also reduced cholinergic neurotransmission in the brain (Morrison and Hof, 1997). The potential involvement of acetylcholinesterase (AChE) in the formation and deposition of extracellular plaques in the human brain of AD patients has been revealed. So far, there is no cure for AD. The main strategy for AD is based on the cholinergic

Electronic supplementary material The online version of this article (doi:10.1007/s00044-016-1648-1) contains supplementary material, which is available to authorized users.

✉ Ayşe Selcen Alpan
selcen.alpan@ege.edu.tr

[1] Department of Pharmaceutical Chemistry, Faculty of Pharmacy, Ege University, Bornova 35100 Izmir, Turkey

[2] Department of Pharmaceutical Chemistry, Institute of Pharmacy, Martin-Luther University of Halle-Wittenberg, Halle/Saale 06120, Germany

Published online: 21 July 2016

hypothesis, which relies on the repair of cognitive and memory deteriorations by elevating the reduced acetylcholine (ACh) (Pan et al., 2014). For this purpose, cholinesterase inhibitors (ChEI) have been used to treat the cognitive and functional symptoms of AD (Weinstock, 1999).

AChE and butyrylcholinesterase (BuChE) are the two types of cholinesterase enzyme. They both play important roles in the regulation of ACh levels and suggested to have a role in the development and progression of AD (Greig et al., 2001). In AD, AChE activity decreases, whereas BuChE activity increases. It is reported in the literature that the elevated BuChE may act as a compensatory mechanism for ACh hydrolysis and ACh regulation may become increasingly dependent on BuChE as AD progresses (Giacobini, 2004; Greig et al., 2002). Due to these findings, it can easily be proposed that BuChE inhibition is also significant for AD treatment.

The difference between BuChE and AChE's active gorge can be demonstrated from the considerably more space present in the gorge cavity of BuChE than that present in AChE. Some of the aromatic residues in AChE are replaced by smaller aliphatic or polar amino acids inside the gorge of BuChE (Galdeano et al., 2010). Compound's selectivity might be due to the fact that the two ChEs differ by the presence of extent of subdomains within the gorge domains (mid-gorge aromatic recognition site), peripheral anionic site, and acyl-binding pocket, even if both ChEs show a similar overall structure (65 % amino sequence homology) and both active sites (CAS) are located inside of a ~20 Å deep gorge cavity (Brus et al., 2014; Nicolet et al., 2003; Cheung et al., 2012).

In our previous study, 2-phenylsubstituted-1*H*-benzimidazole was chosen as a scaffold and basic cyclic, acyclic amino residues were incorporated to this scaffold with ethoxy chain. 5-methyl and 5-chloro benzimidazole derivatives were also synthesized as well as the non-substituted analogs (Alpan et al., 2013). The results indicated that most of the compounds displayed moderate to good AChE inhibition and some of them showed weak to moderate BuChE inhibition. Thus, these activity results revealed selective AChE inhibitors in some of the compounds.

In this study, 2-phenylsubstituted-1*H*-benzimidazole scaffold was conserved, while the position of the ethoxy side chain was moved from para to ortho to obtain more spherical molecules in order to fit in the active gorge of BuChE and improve butyrylcholinesterase inhibitor (BuChEI) activity. Docking studies and molecular dynamics (MD) simulations were carried out to explain the ChEI activity in terms of binding interactions. The reason of the fluctuation between the BuChEI activity results were proposed and discussed by molecular modeling techniques.

Material and methods

Chemistry

Melting points were determined with Electrothermal IA9100 melting point apparatus (Electrothermal, Essex, UK). The infrared (IR) spectra of the compounds were monitored as potassium bromide pellets on Jasco FT/IR-430 (Jasco, Tokyo, Japan) and Perkin-Elmer Spectrum 100 FT-IR spectrometers (PerkinElmer, Waltham, MA, USA). The nuclear magnetic resonance (NMR) spectra (400 MHz for ^{1}H and ^{13}C) were recorded on AS400 Mercury Plus NMR Varian (Varian Inc., Palo Alto, CA, USA) using $CDCl_3$. Chemical shifts were measured in parts per million (δ). The *J* values were given in Hz. Mass spectra were taken on a Thermo Quantum Access Max connected with TSQ quantum high performance liquid chromatography (Thermo Fisher Scientific, San Jose, CA, USA), using ESI (+) method, with C-18 column. Elemental analyses were performed by Leco TruSpec Micro CHNS (Leco, St. Joseph, MI, USA) and were within ±0.4 % of the theoretical values. Compounds **1a**, **1c**, **2b**, and **3e** are reported with fractional mol of water, compounds **2a**, **3a**, **3b**, and **3c** are reported with fractional mol of ethyl acetate, and compound **3d** is reported with fractional mol of methanol. Analytical thin-layer chromatography (TLC) was run on Merck silica gel plates (Kieselgel $60F_{254}$) with detection by ultraviolet (UV) light; column chromatography was performed using Merck silica gel 60 (63–200 mm diameter) and compounds **1b**, **1c**, **1d**, **1e**, **2b**, **2c**, **2d**, and **2e** were eluted with benzene:ethyl acetate:methanol:ammonia (10:2.5:0.5:0.002) and the rest of the synthesized compounds were eluted with toluene:ethyl acetate:methanol:ammonia (10:2.5:0.5:0.002). All starting materials and reagents were of high-grade commercial products.

General procedure for the synthesis of the benzimidazole derivatives

Compounds **1b**, **1c**, **1d**, **1e**, **2b**, **2c**, **2d**, and **2e** are reported derivatives, but corresponding scientific reference data were expanded with elemental analysis (supplementary data) (Coban et al., 2009).

The preparation of the substituted benzimidazoles is outlined in Scheme 1 (Hein et al., 1957; Nagai et al., 1973). 2-(1*H*-benzimidazole-2-yl)phenol, 2-(5-methyl-1*H*-benzimidazole-2-yl)phenol, and 2-(5-chloro-1*H*-benzimidazole-2-yl)phenol were synthesized by reacting *o*-phenylenediamine and sodium hydroxy(2-hydroxyphenyl) methane sulfonate salt as described (Coban et al., 2009). After reacting 0.005 mol of 2-(1*H*-benzimidazole-2-yl)phenol derivatives and 0.01 mol of appropriate *N*-(2-chloroethyl) substituted amine with 0.015 mol of sodium hydroxide in 10 mL

Scheme 1 The synthesis pathway of compounds **1a–e**, **2a–e**, and **3a–e**

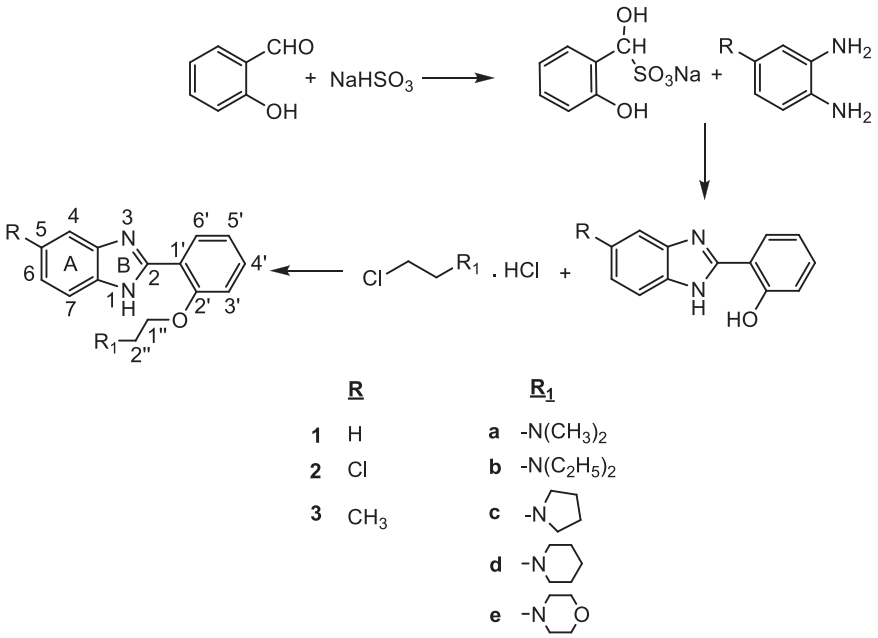

ethanol, the mixture was refluxed at 95 °C for 2 h in an oil bath. Ethanol was evaporated and the residue was extracted with ether. The compounds were purified by column chromatography [benzene:ethyl acetate:methanol:ammonia (10:2.5:0.5:0.002)] and then crystallized with an appropriate solvent.

Structural data of the benzimidazole derivatives

2-[2-(1H-benzo[d]imidazol-2-yl)phenoxy]-N,N-dimethylethanamine (**1a**) White crystalline (MetOH–H_2O). Recrystallized from methanol-water (1:1). Yield: 8.52 %; mp 90 °C; IR ν_{maks} (KBr) cm^{-1}: 3066, 2942, 2774, 1621, 1582, 1468, 1439, 1277, 1245, 1123, 1030, 737. LS MS/MS (ESI^+) *m/z* 282 [M+H, 100]. ^1H NMR (400 MHz, $CDCl_3$) δ 2.48 (6H, s, H-1″′, H-2″′), 2.84 (2H, t, $J = 5.4$ Hz, H-2″), 4.28 (2H, t, $J = 5.2$ Hz, H-1″), 7.03 (1H, d, $J = 8.4$ Hz, H-3′), 7.15 (1H, td, $J = 7.8/0.8$ Hz, H-5′), 7.22–7.24 (2H, m, H-5, H-6), 7.35–7.40 (2H, m, H-4′, H-7), 7.81 (1H, brs, H-4), 8.53 (1H, dd, $J = 8.0/2.0$ Hz, H-6′) ppm. ^{13}C NMR (100 MHz, $CDCl_3$) δ 44.6 (C-1″′), 57.9 (C-2″), 65.9 (C-1″), 114.2 (C-3′), 120.1 (C-1′), 122.0 (C-5′), 122.2 (C-5, C-6), 130.2 (C-6′), 130.7 (C-7a), 150.1 (C-2), 156.3 (C-2′) ppm. Anal. Calcd. for: $C_{17}H_{19}N_3O$ $0.1H_2O$: C, 72.11; H, 6.83; N, 14.84. Found: C, 72.13; H, 6.62; N, 14.66.

2-[2-(5-chloro-1H-benzo[d]imidazol-2-yl)phenoxy]-N,N-dimethylethanamine (**2a**) White crystalline (EtOAc). Recrystallized from ethyl acetate. Yield: 12.84 %; mp 124 °C. IR ν_{maks} (KBr) cm^{-1}: 3200, 2941, 2822, 2773, 1602, 1580, 1462, 1280, 1245, 1121, 1038, 749. LS MS/MS (ESI^+) 316 [M+H, 100], 317 [M+1+H, 21], 318 [M+2+H, 25]. ^1H NMR (400 MHz, $CDCl_3$) δ 2.47 (3H, s, H-1″′ or H-2″′), 2.48 (3H, s, H-1″′ or H-2″′), 2.85 (2H, t, $J = 4.8$ Hz, H-2″), 4.30 (2H, t, $J = 4.8$ Hz, H-1″), 7.01 (1H, dd, $J = 8.0/0.8$ Hz, H-3′), 7.14 (1H, td, $J = 7.6/0.8$ Hz, H-5′), 7.21 (1H, d, $J = 8.0$ Hz, H-6), 7.36 (1H, brs, H-7), 7.40 (1H, t, $J = 7.8/0.8$ Hz, H-4′), 7.69–7.77 (1H, m, H-4), 8.47 (1H, d, $J = 8.0/0.8$ Hz, H-6′) 13.07 (1H, s, N-H) ppm. ^{13}C NMR (100 MHz, $CDCl_3$) δ 44.6 (C-1″′), 57.9 (C-2″), 65.9 (C-1″), 114.2 (C-3′), 118.8 (C-1′), 122.3 (C-5′), 130.3 (C-6′), 131.1 (C-4′), 156.4 (C-2′) ppm. Anal. Calcd. for: $C_{17}H_{18}ClN_3O$ $0.05C_4H_8O_2$: C, 64.52; H, 5.79; N, 13.12. Found: C, 64.73; H, 5.94; N, 12.88.

N,N-dimethyl-2-{2-[5-methyl-1H-benzo[d]imidazol-2-yl] phenoxy}ethanamine (**3a**) Oil. Yield: 13.74 %. IR ν_{maks} (KBr) cm^{-1}: 3171, 2938, 2774, 1629, 1584, 1467, 1273, 1250, 1124, 1040, 802, 762, 749. LS MS/MS (ESI^+) *m/z* 296 [M+H, 100]. ^1H NMR (400 MHz, $CDCl_3$) δ 2.48 (6H, s, H-1″′, H-2″′), 2.49 (3H, s, Ar–CH_3), 2.85 (2H, t, $J = 5.2$ Hz, H-2″), 4.29 (2H, t, $J = 5.4$ Hz, H-1″), 7.04 (1H, d, $J = 7.2$ Hz, H-3′), 7.06 (1H, d, $J = 8.2$ Hz, H-6), 7.14 (1H, td, $J = 7.6/1.2$ Hz, H-5′), 7.35–7.42 (2H, m, H-4′, H-7), 7.52 (1H, brs, H-4), 8.52 (1H, dd, $J = 8.0/2.0$ Hz, H-6′) ppm. ^{13}C NMR (100 MHz, $CDCl_3$) δ 21.8 (Ar–CH_3), 44.6 (C-1″′), 57.9 (C-2″), 65.9 (C-1″), 114.1 (C-3′), 120.2 (C-1′), 122.2 (C-5′), 123.6 (C-6), 130.1 (C-6′), 130.5 (C-4′), 149.8 (C-2), 156.2 (C-2′) ppm. Anal. Calcd. for: $C_{18}H_{21}N_3O$ $0.3C_4H_8O_2$: C, 71.66; H, 7.33; N, 13.06. Found: C, 71.91; H, 7.40; N, 12.90.

N,N-diethyl-2-[2-(5-methyl-1H-benzo[d]imidazol-2-yl)phenoxy]ethanamine (**3b**) Oil. Yield: 17.32 %. IR ν_{maks} (KBr) cm^{-1}: 3188, 2970, 2925, 2853, 1627, 1602, 1585, 1466,

1272, 1242, 1040, 806, 751. LS MS/MS (ESI^+) *m/z* 324[M+H, 100]. ^1H NMR (400 MHz, $CDCl_3$) δ 1.14 (6H, t, J = 7.0 Hz, H-2″′), 2.49 (3H, s, Ar–CH_3), 2.80 (4H, q, J = 7.2 Hz, H-1″′), 2.95 (2H, t, J = 5.2 Hz, H-2″), 4.29 (2H, t, J = 5.2 Hz, H-1″), 7.03–7.07 (2H, m, H-3′, H-6), 7.13 (1H, td, J = 6.8/0.8 Hz, H-5′), 7.37 (2H, m, H-4′, H-7), 7.57 (1H, brs, H-4), 8.52 (1H, dd, J = 7.8/1.6 Hz, H-6′) ppm. ^{13}C NMR (100 MHz, $CDCl_3$) δ 11.0 (C-2″′), 21.8 (Ar–CH_3), 46.4 (C-1″′), 51.3 (C-2″), 65.6 (C-1″), 113.8 (C-3′), 119.9 (C-1′), 122.1 (C-5′), 123.7 (C-6), 130.1 (C-6′), 130.6 (C-4′), 149.8 (C-2), 156.2 (C-2′) ppm. Anal. Calcd. for: $C_{20}H_{25}N_3O$ $0.5C_4H_8O_2$: C, 71.90; H, 7.95; N, 11.43. Found: C, 71.72; H, 7.74; N, 11.34.

5-methyl-2-{2-[2-(pyrrolidin-1-yl)ethoxy]phenyl}-1H-benzo[d]imidazole (**3c**) Oil. Yield: 13.53 %. IR ν_{maks} (KBr) cm^{-1}: 3044, 2962, 2880, 1628, 1603, 1582, 1461, 1278, 1246, 1045, 810, 761, 751. LS MS/MS (ESI^+) *m/z* 322 [M+H, 100]. ^1H NMR (400 MHz, $CDCl_3$) δ 1.88–1.91 (4H, m, H-3″′, H-4″′), 2.49 (3H, s, Ar–CH_3), 2.73 (4H, t, J = 5.6 Hz, H-2″′, H-5″′), 3.00 (2H, t, J = 5.2 Hz, H-2″), 4.28 (2H, t, J = 5.2 Hz, H-1″), 6.99 (1H, d, J = 8.4 Hz, H-3′), 7.06 (1H, dd, J = 8.0/1.2 Hz, H-6), 7.12 (1H, td, J = 7.2/1.0 Hz, H-5′), 7.33–7.38 (2H, m, H-4′, H-7), 7.49 (1H, brs, H-4), 8.47 (1H, dd, J = 7.6/1.6 Hz, H-6′) ppm. ^{13}C NMR (100 MHz, $CDCl_3$) δ 21.8 (Ar–CH_3), 23.8 (C-3″′, C-4″′), 53.3 (C-2″′, C-5″′), 55.0 (C-2″), 67.1 (C-1″), 113.7 (C-3′), 120.0 (C-1′), 122.0 (C-5′), 123.6 (C-6), 130.2 (C-6′), 130.6 (C-4′), 149.9 (C-2), 156.4 (C-2′) ppm. Anal. Calcd. for: $C_{20}H_{23}N_3O$ $0.5C_4H_8O_2$: C, 72.30; H, 7.45; N, 11.50. Found: C, 72.11; H, 7.07; N, 11.77.

5-methyl-2-{2-[2-(piperidin-1-yl)ethoxy]phenyl}-1H-benzo[d]imidazole (**3d**) White crystalline (MetOH–H_2O). Recrystallized from methanol-water (1:1). Yield: 11.67 %; mp 108 °C. IR ν_{maks} (KBr) cm^{-1}: 3274, 2930, 2766, 1627, 1602, 1584, 1462, 1271, 1243, 1121, 1049, 767, 752. LS MS/MS (ESI^+) *m/z* 336 [M+H, 100]. ^1H NMR (400 MHz, $CDCl_3$) δ 1.52 (2H, t, J = 4.8Hz, H-4″′), 1.69 (4H, p, J = 5.6 Hz, H-3″′, H-5″′), 2.50 (3H, s, Ar–CH_3), 2.55 (4H, s, H-2″′, H-6″′), 2.82 (2H, t, J = 5.6 Hz, H-2″), 4.27 (2H, t, J = 5.6 Hz, H-1″), 6.98 (1H, d, J = 8.4 Hz, H-3′), 7.08 (1H, d, J = 7.6 Hz, H-6), 7.12 (1H, td, J = 7.6/0.8 Hz, H-5′), 7.32–7.43 (2H, m, H-4′, H-7), 7.61–7.71 (1H, m, H-4), 8.52 (1H, dd, J = 7.6/1.6 Hz, H-6′) ppm. ^{13}C NMR (100 MHz, $CDCl_3$) δ 21.9 (Ar–CH_3), 24.3 (C-4″′), 25.7 (C-3″′, C-5″′), 54.1 (C-2″), 57.4 (C-2″′, C-6″′), 64.5 (C-1″), 112.9 (C-3′), 119.5 (C-1′), 121.8 (C-5′), 123.7 (C-6), 130.2 (C-6′), 130.7 (C-4′), 150.0 (C-2), 156.1 (C-2′) ppm. Anal. Calcd. for: $C_{21}H_{25}N_3O$ $0.25CH_4O$: C, 74.31; H, 7.63; N, 12.23. Found: C, 74.56; H, 7.71; N, 11.84.

4-{2-[2-(5-methyl-1H-benzo[d]imidazol-2-yl)phenoxy]ethyl}morpholine (**3e**) White crystalline (MetOH–H_2O). Recrystallized from methanol-water (1:1). Yield: 12.48 %; mp 142 °C. IR ν_{maks} (KBr) cm^{-1}: 3355, 2953, 2855, 1625, 1583, 1454, 1275, 1245, 1117, 1036, 767, 750. LS MS/MS (ESI^+) *m/z* 338 [M+H, 100]. ^1H NMR (400 MHz, $CDCl_3$) δ 2.50 (3H, s, Ar–CH_3), 2.65 (4H, t, J = 4.4 Hz, H-2″′, H-6″′), 2.92 (2H, t, J = 5.2 Hz, H-2″), 3.83 (4H, t, J = 4.4 Hz, H-3″′, H-5″′), 4.31 (2H, t, J = 5.6 Hz, H-1″), 7.00 (1H, d, J = 8.0 Hz, H-3′), 7.09 (1H, d, J = 8.4 Hz, H-6), 7.14 (1H, t, J = 7.6 Hz, H-5′), 7.36–7.39 (2H, m, H-4′, H-7), 7.62–7.71 (1H, m, H-4), 8.55 (1H, d, J = 7.8 Hz, H-6′), 11.60–11.69 (1H, m, N–H) ppm. ^{13}C NMR (100 MHz, $CDCl_3$) δ 21.8 (Ar–CH_3), 53.2 (C-2″), 57.3 (C-3″′, C-5″′), 63.7 (C-1″), 66.8 (C-2″′, C-6″′), 112.6 (C-3′), 119.1 (C-1′), 121.9 (C-5′), 123.9 (C-6), 130.1 (C-6′), 130.8 (C-4′), 149.9 (C-2), 155.9 (C-2′) ppm. Anal. Calcd. for: $C_{20}H_{23}N_3O_2$ $0.2H_2O$: C, 70.44; H, 6.92; N, 12.32. Found: C, 70.74; H, 6.73; N, 12.00.

Biological activity assays

AChE E.C.3.1.1.7 (Type VI-S, from electric eel) and BuChE E.C. 3.1.1.8, from equine serum, were purchased from Sigma-Aldrich (Steinheim, Germany). 5,5′-dithiobis (2-nitrobenzoic acid) (DTNB)-Ellman's reagent, buffer compounds (potassium dihydrogen phosphate, potassium hydroxide), sodium hydrogen carbonate, and acetylthiocholine iodide (ATC) used as a substrate were obtained from Fluka (Buchs, Switzerland). Spectrophotometric measurements were performed on a Shimadzu UV/160-A spectrophotometer.

AChE/BuChE activity assay

Enzyme activity was investigated using a slightly modified colorimetric method of Ellman et al. (1961). As the product of the enzymatic hydrolysis, the thiocholine does not possess a significant chromophore for UV detection, the evaluation of enzyme activity was performed using a specific chromogenic reagent, DTNB.

Stock solutions of the inhibitor compounds were prepared in 2 % dimethylsulfoxide (DMSO), which were diluted with aqueous assay medium to a final content of organic solvent always lower than 0.2 %. The enzyme activity was determined in the presence of at least five different concentrations of an inhibitor, generally between 10^{-3} and 10^{-8}, in order to obtain the inhibition of AChE or BuChE activity between 0 and 100 %. Each concentration was assayed in triplicate. Prior to use, all solutions were adjusted to 20 °C. Enzyme solution (2.5 units/mL, 100 µL) and inhibitor solution (100 µL) were added into a cuvette containing the phosphate buffer (3.0 mL, 0.1 M; pH = 8.0). After 5 min of incubation, required aliquots of the DTNB solution (0.01 M, 100 mL) and of the ATC (0.075 M, 20 µL)

were added. After a rapid and immediate mixing, the absorption was measured at 412 nm. In vitro BuChE assay was similar with the method described above (Kapková et al., 2013).

Docking studies

The eqBuChE model generated was subjected to energy minimization using AMBER99 force field already implemented in MOE2013.08 software (Molecular Operating Environment Chemical Computing Group Inc., Canada) (Molecular Operating Environment (MOE) 2013.08, 2006). All the ligands were drawn using MOE2013.08, then they were 3D protonated and the partial charges were added using MMFF94× force field. Finally they were minimized using MMFF94× force field within MOE2013. All the docking results were carried out using GOLD5.2 software with default settings (Jones et al., 1997). A sphere of 20 Å around the imidazole group of His438 was selected as binding site, and for every ligand 100 poses were retrained. To score the poses generated, GoldScore and ChemScore were the selected scoring functions.

MD simulations

All the MD simulations presented here have been obtained with AMBER12 (Case et al., 2012). The eqBuChE model was protonated and parameterized using ff99SB force field, whereas all the small compounds were parameterized with *Gaff* force field using the selected docking poses as starting geometries (Case et al., 2012; Wang et al., 2004). The atom types and partial charges of the ligands were added using *antechamber* module, whereas the missing *Gaff* force field parameters were generated using *parmchk* module, both implemented in AMBER suite. The complexes were then generated with *Leap* module from AMBER. Subsequently, every complex, formed by the protein and small ligand, was neutralized adding six Cl-counterions and solvated in octahedral box using TIP3P water molecules leaving at least 12.0 Å between the solute atoms and the border of the box (~17,062 water molecules were added for every complex). Several systems were generated, according to the hypotheses of binding found. Every complex was formed by ~59,691 atoms (Case et al., 2012; Jorgensen et al., 1983). Finally the MDs were conducted using *sander* program implemented in AMBER suite (Case et al., 2012).

In order to remove bad close contacts, every starting system was initially relaxed in three steps. During the first step, counterions and water molecules were relaxed for 800 iterations using steepest descent gradient and for 800 iterations using conjugate gradient, while the solute was constrained with a positional restraint by a force of 10 Kcal/mol/Å. During the second step, only the ligand was constrained on its starting geometries, while the solvent and the protein were relaxed again with 800 iterations steepest descent gradient and 800 iterations conjugate gradient methods. In the last relaxation step, all constrains were removed and the whole system was minimized for 1000 iterations using steepest descent gradient and 1000 iterations using conjugate gradient methods. Following the relaxation steps every system generated was then gradually heated until 300 K within 300 ps of MD using positional restraint for the atoms belonging to the solute (10 Kcal/mol/Å). The solvent and the counterions were allowed to move freely. To equilibrate the temperature, a constant volume periodic boundary was set on the systems by Langevin dynamics setting a collision frequency of 1.0 ps^{-1} (Pastor et al., 1988). After the temperature was equilibrated, every system previously generated was subjected to pressure equilibration of 1 bar for 300 ps in constant pressure periodic boundary by an isotropic pressure scaling method employing a pressure relaxation time of 2.0 ps, while the temperature was kept set on 300 K by the Langevin dynamics. In this step the solute was constrained with a positional restrains like in the heating step.

After an equilibration step in which the positional constrains were gradually removed (at 300 K temperature and 1 bar pressure), the systems generated were subjected to 40 ns MD simulation. For all the equilibration and the free MD steps, 8 Å was the cutoff selected for the short-range non-bonded interactions in combination with the Particle Mesh Ewald option (Darden et al., 1993), while the length of the hydrogen atoms covalently bounded to heteroatoms were kept constant through *shake* method (Hornak et al., 2006). Coordination's and energy parameters were saved every 100 iterations during the relaxation steps, every 400 iterations during the temperature and pressure equilibration steps, and every 4000 iterations during the MD simulations. Visual molecular dynamics (VMD) was used for visualization of the trajectories, whereas PYMOL [The PYMOL Molecular Graphics System, Version 1.5.0.4 Schrödinger, LLC] was used for the preparation of the figures (Humphrey et al., 1996).

Results and discussion

Chemistry

1*H*-benzimidazole derivatives were synthesized by the reported methods in the literature (Scheme 1) (Coban et al., 2009).

The structures of title compounds were verified by spectral (IR, ^{1}H NMR, ^{13}C NMR, and ESI-Mass) and elemental analysis. In the IR spectra of the title compounds, the characteristic frequencies for benzimidazole derivatives

and aryl-alkylethers were observed between 2400–3300 cm^{-1} and 1030–1250 cm^{-1}, respectively (Hesse et al., 1997). The assessment of the chemical shifts in ^{1}H NMR spectra demonstrated that aromatic and aliphatic protons were observed in the expected regions confirming the substitution patterns. The aromatic proton signals of the side chain at 2-position were observed within prospective chemical shift values and divisions, while the some of the protons of 1*H*-benzimidazole ring at 4- and 7-positions were not detected at the prospective divisions. The lack of H atom signals on ^{1}H NMR spectra and the lack of the signals belonging to **3a**, **4**, **7**, and **7a** C atoms in ^{13}C NMR spectra are noteworthy as it may suggest a proton exchange due to 1,3-tautomerization (Sridharan et al., 2005). NMR spectral results were assigned by using the 2D HSQC and HMBC techniques. The mass spectra of the title compounds were recorded in respect to the positive ion mode electrospray ionization (ESI+) technique. The $[M+H]^{+}$ ions of title compounds compromised with the calculated molecular weights. The definitions are inserted in the abbreviation part but we couldn't set the line format. The visual of the abbreviation part must be checked.

Biological study

ChEI activities of the target compounds were tested by spectrophotometric method of Ellman et al. and tacrine was used as the reference compound (Ellman et al., 1961). Evaluation of the enzyme activity was performed using a specific chromogenic reagent, 5,5′-dithiobis(2-nitrobenzoicacid), known as Ellman's reagent, with the sulfhydryl group of acetylthiocholine or butyrylthiocholine which result as a yellow-colored product, that is, 2-nitro-5-thiobenzoic acid. The activity was determined by measuring the increase in absorbance at 412 nm at 5 min intervals at 20 °C. IC_{50} values of the title compounds are summarized in Table 1. According to the biological activity results, all compounds exhibited moderate inhibitory activity against AChE and most of the compounds displayed good inhibitory activities against BuChE. Moreover most of the compounds possessed selectivity against BuChE.

Regarding BuChEI activity, compounds bearing diethyl group, pyrrolidine, and piperidine rings on terminal nitrogen displayed high inhibition, whereas compounds bearing dimethyl group and morpholine ring gave poor inhibition values. When IC_{50} values of the compounds bearing diethyl substituents were compared to its cyclized analog pyrrolidine, similar IC_{50} values were determined, but when 5-C ring was replaced with 6-C ring (piperidine), the inhibition increased. On the contrary, a sharp decrease in BuChE inhibition was observed with the alteration of the piperidine ring to its isostere, i.e., morpholine. When each group (**1**, **2**, **3**) was evaluated within themselves, the lowest activity was observed in the derivatives with dimethyl groups at terminal nitrogen (**1a**, **2a**, **3a** $IC_{50} = 7.02$, 100, 56.31 μM, respectively). Additionally, substitutions at 5-position of the benzimidazole ring did not provide a significant change in the biological activity.

In respect to AChE activity results, all compounds displayed inhibitory activity with IC_{50} values ranging from

Table 1 In vitro inhibition of AChE/BuChE and calculated log *P* vaules

	$IC_{50} \pm SEM$ (μM)[a]			
	AChE	BChE	Selectivity BChE/AChE	Log *P*[b]
1a	14.03 ± 0.38	7.02 ± 0.51	2	3.11
1b	15.35 ± 0.41	1.09 ± 0.08	14.08	3.80
1c	9.40 ± 0.20	1.02 ± 0.04	9.22	3.65
1d	14.44 ± 0.31	0.37 ± 0.02	38.92	4.09
1e	8.79 ± 0.36	3.98 ± 0.42	2.21	2.68
2a	19.35 ± 0.50	> 100		3.74
2b	11.35 ± 0.54	0.66 ± 0.06	17.20	4.24
2c	10.52 ± 0.23	0.90 ± 0.10	11.69	4.27
2d	13.22 ± 0.27	0.83 ± 0.05	15.93	4.72
2e	12.30 ± 0.29	19.04 ± 0.47	0.65	3.31
3a	13.32 ± 0.42	56.31 ± 2.90	0.23	3.45
3b	14.58 ± 0.49	0.69 ± 0.01	21.13	4.13
3c	14.73 ± 0.21	0.56 ± 0.03	26.30	3.98
3d	14.87 ± 2.82	0.23 ± 0.01	64.65	4.42
3e	12.07 ± 0.29	19.51 ± 0.35	0.62	3.01
Tacrine	0.075 ± 0.02	0.0098 ± 0.0002	–	–

[a] Data are means ± standard error of the mean of triplicate independent experiments

[b] Log *P* calculated using MOE 2013.08

8.79 to 19.35 μM. These results indicated that the positional change from para to ortho lead to a decrease in the inhibitory activity compared to our previous study.

Log *P* values of all the benzimidazole derivatives were calculated by using MOE 2013.08 program and were between 2.68 and 4.72. The compounds with log *P* values of approximately 4 exhibited the best inhibitory activity against BuChE. These values support the idea that all of the compounds might penetrate blood brain barrier.

Overall, compound **3d** with IC_{50} value of 0.23 μM presented a noteworthy BuChE inhibitory activity compared to the reference, tacrine ($IC_{50} = 0.0098$ μM) and is reported as the most selective BuChE inhibitor compound in the series (BuChE/AChE = 64.65).

Computational studies

Docking studies and MD simulations were conducted in order to predict the interactions of the title compounds inside eqBuChE and to describe the selectivity for BuChE over AChE (Alpan et al., 2013). From the lack of eqBuChE X-ray crystal structure, a homology model was initially generated. The model was obtained through SWISS-MODEL server using a default automatized pipeline (Arnold et al., 2006; Benkert et al., 2011). The three-dimensional geometries of eqBuChE were obtained after primary sequences alignment with huBuChE X-ray crystal structure (2PM8.pdb) that shows a primary sequence identity of 89.79 % with eqBuChE.

Consequently, all the compounds belonging to the data set were processed to docking studies. Several hypotheses of binding were selected according to GoldScore scoring function and through visual inspection.

In order to choose the putative binding mode among the results obtained through docking technique, for the most active derivative (**3d**), several MD simulations were carried out according to its most promising hypotheses of binding. Only one binding mode showed high stability inside the binding cavity of the enzyme without losing the key interactions found by the docking (Fig. 1). For this reason it was selected as the putative one (the MD simulations of the hypotheses of binding discarded are reported in the supporting information).

According to the binding hypothesis selected, the new benzimidazole derivatives interact inside eqBuChE binding cavity in the same region occupied by tacrine co-crystalized with huBuChE (4BDS.pdb) (Fig. 2). Here the compounds find interactions in the middle of the active-site gorge and partially to the CAS (Fig. 2) (Alpan et al., 2013). The main protein–ligand interactions are reproduced when compared to tacrine-binding interactions inside huBuChE crystal structure (Galdeano et al., 2010; Nachon et al., 2013). A π–π aromatic stack of the benzimidazole group (present in every compound) with the side chain of Trp82 and a putative hydrogen bond interaction between the benzimidazole nitrogen (when protonated) and the carbonyl group of His438 backbone (Figs. 1 and 2). Moreover all the compounds are showing a positively charged nitrogen atom that can find an intermolecular interaction with the non-protonated nitrogen atom of the benzimidazole group (Fig. 1).

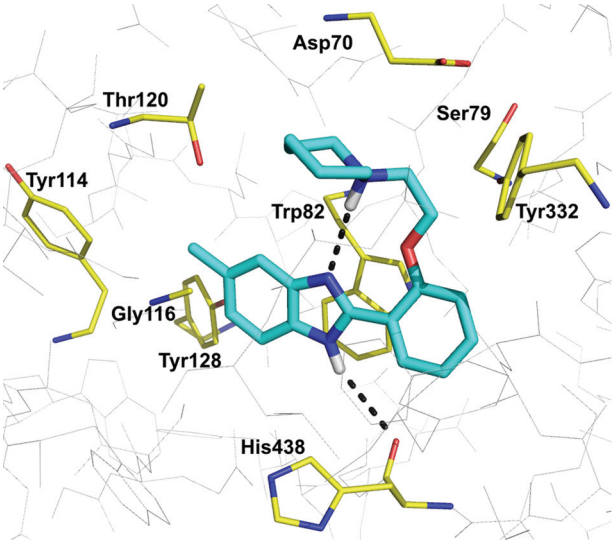

Fig. 1 Proposed binding mode for compound **3d** inside eqBuChE model. The active compound is showed as sticks and colored *cyan*. The most involved residues are named using three letters code and showed as *yellow* sticks. The hydrogen interactions are represented as *black dashed* lines, while only polar hydrogen atoms belonging to the ligand are showed for clarity

The MD of the putative binding mode for compound **3d** revealed high stability for the whole MD length (42 ns), suggesting conserved interactions inside gorge cavity of eqBuChE protein (supporting information). The average root main square deviation (RMSD) value of the ligand increases to ~2.60 Å in the first part of the MD without losing the key interactions found through docking studies when compared to the starting conformation. After ~27 ns the ligand is moving back to its starting geometries showing a RMSD value of ~1.80 Å, when compared to its starting conformation, until the end of the MD. The average RMSD value of the protein reaches the steady state around 1.80 Å, suggesting small deviation from the starting binding geometries within 42 ns of MD (supporting information).

Furthermore in order to describe the reduced activity of some compounds present in the database, also **3a** and **3e** derivatives were processed to MD simulations following the geometries of binding of the putative binding mode found (supporting information). According to the MD simulations conducted, the weak activity of compounds **3a** and **3e**, with an IC_{50} of 19.51 μM and 56.31 μM, respectively, may be

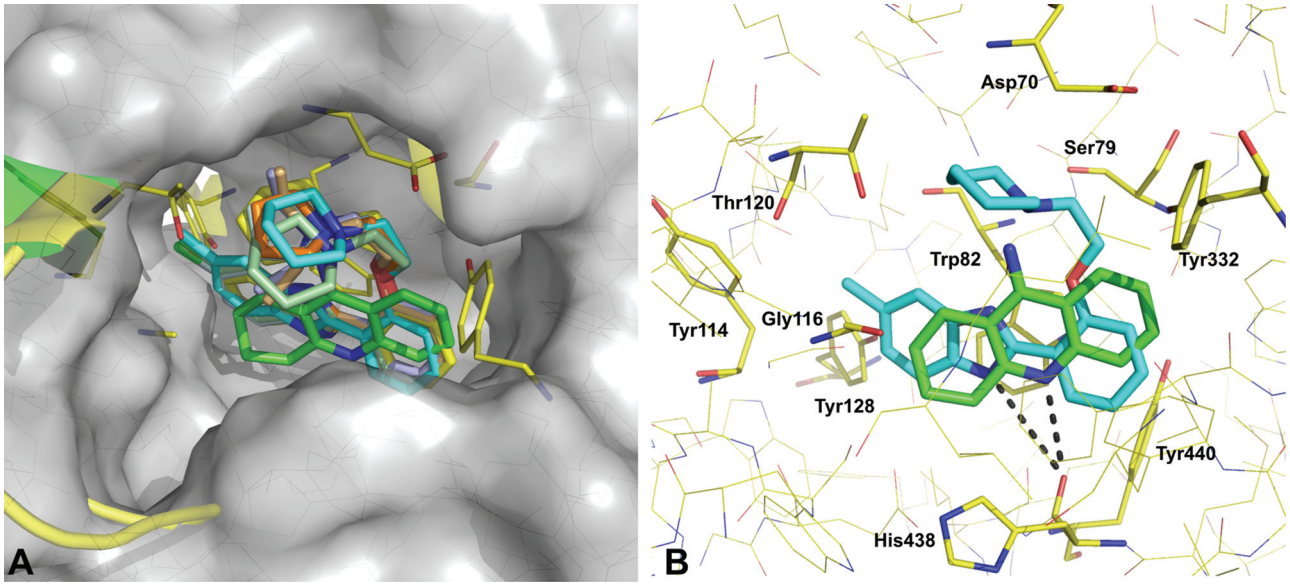

Fig. 2 **a** External surface with gorge cavity of eqBuChE showing the proposed binding mode for **3d**, **2d**, **1d**, **3c**, **2c**, **3b**, and **2b** active compounds superimposed with the binding mode showed by tacrine inside huBuChE crystal structure (4BDS.pdb). **3d** compound is showed as *cyan* sticks, while **2d**, **1d**, **3c**, **2c**, **3b**, **2b**, and tacrine are showed as *pale green*, *yellow*, *orange*, *pale cyan*, *light orange*, *light blue*, and *green* sticks, respectively. The proteins surface is showed *gray*, while the most involved residues are colored as *yellow* sticks. The protein is showed as *yellow* ribbons. **b** Proposed binding mode for **3d** active compound inside gorge cavity of eqBuChE superimposed with the binding mode showed by tacrine inside huBuChE crystal structure (4BDS.pdb). **3d** is colored as *cyan* sticks, tacrine is showed as *green* sticks, while the involved residues are named using three letters code and colored as *yellow* sticks. Protein–ligand hydrogen interactions are represented as *black dashed* lines, while hydrogen atoms are omitted for clarity

due to their higher instability inside the eqBuChE protein (supporting information).

The activity differences among the three series of the title compounds present in the data set might also be partially explained with the computational models obtained. Indeed, substitutions at position 5 of the benzimidazole ring fill up a hydrophobic subpocket (Tyr128, Tyr114, Gly116, and Thr120) of eqBuChE active-site gorge cavity (Figs. 1 and 2).

Finally the selectivity showed by this new data set for BuChE over AChE is explained from the considerably more space present in the gorge cavity of BuChE than that present in AChE. This reflect the fact that 6 out of 14 aromatic residues present in the huAChE gorge cavity (Tyr72, Tyr124, Trp286, Phe295, Phe297, and Tyr337) are replaced by smaller aliphatic or polar amino acids inside the gorge of huBuChE [Asn68, Gln119, Ala277 (Val277 inside eqBuChE), Leu286, Val288, and Ala328] (Galdeano et al., 2010) (Fig. 3).

Conclusion

It can be concluded that according to the studies conducted here and in the previous article, substitution from *p*-[aminoethoxy]phenylbenzimidazole derivatives to *o*-[aminoethoxy]phenylbenzimidazole derivatives, the activity of the title compounds switches from AChE to BuChE (Alpan et al., 2013). Also, different substitutions both on the benzimidazole ring did not exhibit any noticeably change on ChE inhibitor activity potency. The activity shift to BuChE is reasonable since in literature is already demonstrated how compounds may adopt different geometries of binding inside AChE and BuChE due to volume differences inside their respectively active-site gorge cavities (Galdeano et al., 2010; Silva et al., 2013; Bautista-Aguilera et al., 2014). Figure 3 clearly shows the steric clashes that can occur with the side chain of Tyr337 (Ala328 in eqBuChE) when the active compounds interact inside huAChE gorge cavity adopting the geometries of binding found inside BuChE. Moreover the flexibility of the groups bounded to the amino terminal group linked to the ethoxyphenyl spacer at position 2 of the benzimidazole ring it modifies the activity of the compounds when tested on BuChE. Here, bulky, nonflexible, and a polar substitutions are favoured. Through the modeling studies described, synthesis of new promising derivatives is in progress in order to obtain less flexible derivatives able to strongly interact inside the active-site gorge cavities of BuChE.

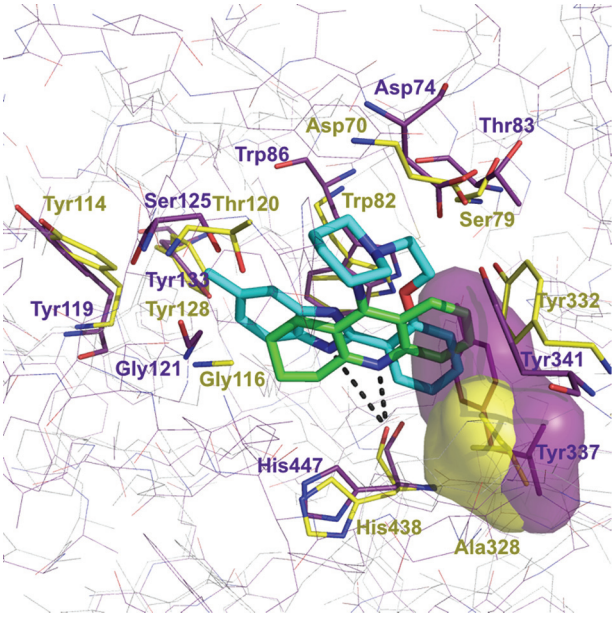

Fig. 3 Superimposition of huAchE crystal structure (4EY7.pdb) with eqBuChE model showing inside the gorge cavity the proposed binding mode of **3d** active compound and tacrine according to the geometries of binding inside huBuChE crystal structure (4BDS.pdb). **3d** is showed as *cyan* sticks, while tacrine is showed as *green* sticks. The involved residues regarding eqBuChE are showed as *yellow* sticks and named using three letters code. The involved residues concerning huAchE are showed as *purple* sticks and named using three letters code. For Tyr337 and Ala328 also the surface is showed as *purple* and *yellow*, respectively. Protein–ligand interactions are showed as *black dashed* lines, while hydrogen atoms are omitted for clarity

Supporting information

Docking results

The docking studies were conducted with GOLD5.2 software using GoldScore and ChemScore as scoring functions. Several poses were considered as putative binding modes from the docking studies carried out. Most of them were discarded according to the score values, while some of them were discarded after their instability was confirmed through MD simulations. Since ChemScore was not able to find a reasonable binding mode for all the compounds present in the data set, only the GoldScore values and their absolute ranking position for the docked compounds according the putative binding mode are reported in Supplementary Table S1.

MD simulations

The MD simulations carried out allowed discriminating putative binding modes among several-selected hypothesis of binding obtained through docking studies (Supplementary Figure S1). The starting conformation geometries of the ligands were obtained from the docking studies, while the protein was obtained through homology modeling using huBuChE crystal structure (2PM8.pdb) as a template. After that, the complexes protein–ligand were generated with AMBER12 and subjected to MD simulations. In Supplementary Figure S1 are represented 42 ns RMSD of three promising binding modes found through docking studies. From the RMSD plot, it is clear that only one putative binding mode (red trace) was able to keep the starting geometries of binding inside eqBuCHE model for 42 ns and for this reason it was selected as a putative binding mode (Supplementary Figure S1).

Moreover, MD simulations also allowed describing the activity for some of the less active compounds present in the database (Supplementary Figure S2). Compounds **3a** and **3e** were also simulated inside eqBuChE according to the binding mode found. In Supplementary Figure S2 is represented the RMSD plot of the two moderate active compounds present in the database and compared to the RMSD of **3d** active compound. The purple trace is coupled to the **3a**, the dark green trace is coupled to **3e**, while the red trace is still representing the **3d** movements inside eqBuChE. According to the binding mode found, compounds **3a** and **3e** are not able to show the key interactions inside gorge cavity of eqBuChE for neither 20 ns MD simulation, which are in accordance to their low-activity values. In case of compound **3a**, its reduced activity might be due to the lack of bulky groups on the terminal nitrogen (*o*-dimethylaminoethoxyphenyl substituent). The dimethyl group on the terminal nitrogen highly decreases the hydrophobic contacts to the gorge cavity resulting in more flexible compound when compared to more active inhibitors present in the data set and causes huge movements inside the gorge cavity of eqBuChE promoting loss of the starting key interactions (Supplementary Figure S2). The RMSD plot regarding **3a** is increasing until ~6 Å when compared to the starting conformation before finding the steady state in which the key interactions with eqBuChE are disrupted.

Acknowledgments This study was partially supported by TUBITAK (Turkish Scientific and Technical Research Council) (Project number: 213S027). We appreciate the support of Professor Dr. Wolfgang Sippl for molecular modeling studies. We also thank the Medicinal Chemistry Department of Martin Luther University Institute of Pharmacy and also Pharmaceutical Sciences Research Centre (FABAL) of Ege University Faculty of Pharmacy for equipmental support.

Compliance with ethical standards

Conflict of interest The authors declare that they have no conflict of interest.

References

Alpan AS, Parlar S, Carlino L, Tarikogullari AH, Alptüzün V, Güneş HS (2013) Synthesis, biological activity and molecular modeling studies on 1*H*-benzimidazole derivatives as acetylcholinesterase inhibitors. Bioorg Med Chem 21:4928–4937

Arnold K, Bordoli L, Kopp J, Schwede T (2006) The SWISS-MODEL workspace: a web-based environment for protein structure homology modelling. Bioinformatics 22:195–201

Bautista-Aguilera OM, Esteban G, Bolea I, Nikolic K, Agbaba B, Moraleda I, Iriepa I, Samadi A, Soriano E, Unzeta M, Marco-Contelles J (2014) Design, synthesis, pharmacological evaluation, QSAR analysis, molecular modeling and ADMET of novel donepezil-indolyl hybrids as multipotent cholinesterase/monoamine oxidase inhibitors for the potential treatment of Alzheimer's disease. Eur J Med Chem 75:82–95

Benkert P, Biasini M, Schwede T (2011) Toward the estimation of the absolute quality of individual protein structure models. Bioinformatics 27:343–350

Brus B, Košak U, Turk S, Pišlar A, Coquelle N, Kos J, Stojan J, Colletier J, Gobec S (2014) Discovery, biological evaluation and crystal structure of a novel nanomolar selective butyrylcholinesterase inhibitor. J Med Chem 57(19):8167–8179

Case DA, Darden TA, Cheatham TE, Simmerling CL, Wang J, Duke RE, Luo R, Walker RC, Zhang W, Merz KM, Roberts B, Hayik S, Roitberg A, Seabra G, Swails J, Goetz AW, Kolossv$\hat{a}$ry I, Wong KF, Paesani F, Vanicek J, Wolf RM, Liu J, Wu X, Brozell SR, Steinbrecher T, Gohlke H, Cai Q, Ye X, Wang J, Hsieh MJ, Cui G, Roe DR, Mathews DH, Seetin MG, Salomon-Ferrer R, Sagui C, Babin V, Luchko T, Gusarov S, Kovalenko A, Kollman PA (2012) Amber 12. University of California, San Francisco

Cheung J, Rudolph MJ, Burshteyn F, Cassidy MS, Gary EN, Love J, Franklin MC, Height J (2012) Structures of human acetylcholinesterase in complex with pharmacologically important ligands. J Med Chem 55:10282–10286

Coban G, Zencir S, Zupko´ I, Re´thy B, Gunes HS, Topcu Z (2009) Synthesis and biological activity evaluation of 1*H*-benzimidazoles via mammalian DNA topoisomerase I and cytostaticity assays. Eur J Med Chem 44:2280–2285

Darden T, York D, Pedersen L (1993) Particle mesh Ewald: an N·log (N) method for Ewald sums in large systems. J Chem Phys 98:10089–10092

Ellman GL, Courtney KD, Andres V, Featherstone RM (1961) A new and rapid colorimetric determination of acetylcholinesterase activity. Biochem Pharmacol 7:88–90

Galdeano C, Viayna E, Arroyo P, Bidon-Chanal A, Blas JR, Muñoz-Torrero D, Luque FJ (2010) Structural determinants of the multifunctional profile of dual binding site acetylcholinesterase inhibitors as anti-Alzheimer agents. Curr Pharm Des 16:2818–2836

Giacobini E (2004) Cholinesterase inhibitors: new roles and therapeutic alternatives. Pharmacol Res 50:433–440

Greig NH, Lahiri DK, Sambamurti K (2002) Butyrylcholinesterase: an important new target in Alzheimer's disease therapy. Int Psychogeriatr 14(Suppl. 1):77–91

Greig NH, Utsuki T, Yu Q, Zhu X, Holloway HW, Perry T, Lee B, Ingram DK, Lahiri DK (2001) A new therapeutic target in Alzheimer's disease treatment: attention to butyrylcholinesterase. Curr Med Res Opin 17:159–165

Han S, Mook-Jung I (2014) Diverse molecular targets for therapeutic strategies in Alzheimer's disease. J Korean Med Sci 29: 893–902

Hein DW, Alheim RJ, Leavitt JJ (1957) The use of polyphosphoric acid in the synthesis of 2-aryl- and 2-alkyl-substituted benzimidazoles, benzoxazoles and benzothiazoles. J Am Chem Soc 79 (2):427–429

Hesse M, Meier H, Zeeh B (1997) Spectroscopic methods in organic chemistry, 1st edn. Georg Thieme Verlag, New York

Hornak V, Abel R, Okur A, Strockbine B, Roitberg A, Simmerling C (2006) Comparison of multiple Amber force fields and development of improved protein backbone parameters. Proteins 65:712–725

Humphrey W, Dalke A, Schulten K (1996) VMD—visual molecular dynamics. J Mol Graph 14:33–38

Jones G, Willett P, Glen RC, Leach R, Taylor R (1997) Development and validation of a genetic algorithm for flexible docking. J Mol Biol 267:727–748

Jorgensen WL, Chandrasekhar J, Madura JD (1983) Comparison of simple potential functions for simulating liquid water. J Chem Phys 79:926–935

Kapková P, Stiefl N, Süríg U, Engels B, Baumann K, Holzgrabe U (2013) Synthesis, biological activity and docking studies of new acetylcholinesterase inhibitors of bispyrdinium type. Arch Pharm (Weinheim) 336:523–540

Molecular Operating Environment (MOE) 2013.08. (2006) Chemical Computing Group Inc., Montreal, Quebec, Canada

Morrison JH, Hof PR (1997) Life and death of neurons in the aging brain. Science 278:412–419

Nachon F, Carletti E, Ronco C, Trovaslet M, Nicolet Y, Jean L, Renard PY (2013) Crystal structures of human cholinesterases in complex with huprine W and tacrine: elements of specificity for anti-Alzheimer's drugs targeting acetyl- and butyryl-cholinesterase. Biochem J 453:393–399

Nagai T, Fukushima Y, Kuroda T, Shimizu H, Sekiguchi S, Matsu H (1973) Rearrangement of 2-aryloxybenzazoles. Bull Chem Soc Jpn 46:2600–2602

Nicolet Y, Lockridge O, Masson P, Fontecilla-Camps JC, Nachon F (2003) Crystal structure of human butyrylcholinesterase and of its complexes with substrate and products. J Biol Chem 278:41141–41147

Pan L, Wang X, Xie S, Li S, Kong L (2014) Multitarget-directed resveratrol derivatives: anti-cholinesterases, anti-β-amyloid aggregation and monoamine oxidase inhibition properties against Alzheimer's disease. Med Chem Commun 5:609–616

Pastor RW, Brooks BR, Szabo A (1988) An analysis of the accuracy of Langevin and molecular dynamics algorithms. Mol Phys 65:1409–1419

Silva D, Chioua M, Samadi A, Agostinho P, Garção P, Lajarín-Cuesta R, de los Ríos C, Iriepa I, Moraleda I, Gonzalez-Lafuente L, Mendes E (2013) Synthesis, pharmacological assessment, and molecular modeling of acetylcholinesterase/butyrylcholinesterase inhibitors: effect against amyloid-β-induced neurotoxicity. ACS Chem Neurosci 4(4):547–565

Sridharan V, Saravanan S, Muthusubramanian S, Sivasubramanian S (2005) NMR investigation of hydrogen bonding and 1,3-tautomerism in 2-(2-hydroxy-5-substituted-aryl)benzimidazoles. Magn Reson Chem 43:551–556

Thies W, Bleiler L (2013) Alzheimer's association. 2013 Alzheimer's disease facts and figures. Alzheimers Dement 9:208–245

Wang J, Wolf RM, Caldwell JW, Kollman PA, Case DA (2004) Development and testing of a general amber force field. J Comput Chem 25:1157–1174

Weinstock M (1999) Selectivity of cholinesterase inhibition: clinical implications for the treatment of Alzheimer's disease. CNS Drugs 12:307–323